Low-Level Endogenous PSMA Expression in Nonprostatic Tumor Xenografts Is Sufficient for In Vivo Tumor Targeting and Imaging

Sridhar Nimmagadda[1,2], Mrudula Pullambhatla[1], Ying Chen[1], Princy Parsana[3], Ala Lisok[1], Samit Chatterjee[1], Ronnie Mease[1,2], Steven P. Rowe[1], Shawn Lupold[2,4], Kenneth J. Pienta[2,4], and Martin G. Pomper[1,2,4]

[1]Russell H. Morgan Department of Radiology and Radiological Science, Johns Hopkins Medical Institutions, Baltimore, Maryland; [2]Sidney Kimmel Comprehensive Cancer Center, Johns Hopkins Medical Institutions, Baltimore, Maryland; [3]Department of Computer Science, Johns Hopkins Medical Institutions, Baltimore, Maryland; and [4]James Buchanan Brady Urological Institute and Department of Urology, Johns Hopkins Medical Institutions, Baltimore, Maryland

Prostate-specific membrane antigen (PSMA) is highly expressed in prostate cancer and within the neovasculature of other solid tumors. The nonprostatic expression of PSMA has been reported exclusively within the neovasculature endothelial cells of nonprostatic cancers; however, there are few reports on PSMA expression in epithelial cells. Herein, we describe PSMA expression in nonprostatic epithelial cells and characterize the potential of PSMA-binding agents to noninvasively detect that expression. **Methods:** PSMA expression data were extracted from publicly available genomic databases. Genomic data were experimentally validated for PSMA expression—by quantitative reverse transcription polymerase chain reaction, flow cytometry, and Western blotting—in several nonprostatic cell lines and xenografts of melanoma and small cell lung cancer (SCLC) origin. The feasibility of PSMA detection in those tumor models was further established using PSMA-based nuclear and optical imaging agents and by biodistribution, blocking, and ex vivo molecular characterization studies. **Results:** We discovered that a small percentage of nonprostatic cancer cell lines and tumors express PSMA. Importantly, PSMA expression was sufficiently high to image established melanoma and SCLC xenografts using PSMA-based nuclear and optical imaging agents. **Conclusion:** These results indicate that PSMA expression in nonprostatic tumors may not be limited to the endothelium but may also include solid tumor tissue of nonprostatic cancers including melanoma and SCLC. Our observations indicate broader applicability of PSMA-targeted imaging and therapeutics.

Key Words: prostate cancer; melanoma; lung cancer; molecular imaging; CCLE; TCGA

J Nucl Med 2018; 59:486–493
DOI: 10.2967/jnumed.117.191221

Prostate-specific membrane antigen (PSMA), also known as folate hydrolase (FOLH1) or glutamate carboxypeptidase II, is a type 2 integral membrane protein with zinc-dependent exopeptidase activity (*1,2*). PSMA expression in healthy human tissues is present within the secretory-acinar epithelium of the prostate, proximal tubules of the kidney, astrocytes and Schwann cells of the nervous system, salivary glands, ovaries, and testes (*3*). In prostate cancer, elevated PSMA expression and alternative splicing produce high levels of PSMA protein on the surface of prostate cancer cells. Nearly 95% of prostate cancers are reported to have elevated PSMA expression (*4,5*). Over the past decade, PSMA has gained considerable attention as an imaging and therapeutic target because of its elevated expression within malignant prostate tissues, its presentation on the cell surface, and its rapid cellular internalization kinetics (*6*).

PSMA expression on the endothelial cells of tumor-associated neovasculature has been described in nonprostatic cancers, but its expression on epithelial cells has not been well characterized (*7,8*). Our analysis of large-scale cancer cell line–derived genomic datasets revealed the presence of PSMA in many nonprostatic cancer cell lines, and this finding was corroborated by transcript levels observed in human tumors. We then sought to experimentally validate those observations by in vitro and in vivo characterization of PSMA expression in multiple cancer cell lines and the corresponding tumor xenografts. We also evaluated the potential of existing PSMA-targeted imaging agents to noninvasively assess PSMA expression in tumor xenografts derived from those cell lines. Our results in several tumor models of melanoma and small cell lung cancer (SCLC) origin demonstrate that PSMA expression in nonprostatic epithelial cancer cells is sufficiently high to be detected using SPECT and near-infrared imaging methods. Our results support the view that PSMA-based imaging agents and therapeutics could have much broader applicability by enabling management of nonprostate tumors.

MATERIALS AND METHODS

Analysis of Cancer Cell Line Encyclopedia (CCLE) Database and Cancer Genome Atlas (TCGA) Data

Messenger RNA (mRNA) expression data, in log 2 counts, were downloaded from the CCLE database and converted to z scores using all the cell lines as a reference population. Upper-quartile–normalized RSEM software count estimates of RNA-Seq version 2 data were downloaded for 19 cancer types from the TCGA. FOLH1 gene counts were extracted for these cancer types and converted to log 2 counts. Samples with missing values and "not-a-numbers" were eliminated. Gene expression analysis was performed using the R statistical programming environment. The results presented here are based on data generated by the TCGA Research Network.

Received Feb. 2, 2017; revision accepted Sep. 27, 2017.
For correspondence or reprints contact: Sridhar Nimmagadda, Johns Hopkins Medical Institutions, 1550 Orleans St., CRB II, #491, Baltimore, MD 21287.
E-mail: snimmag1@jhmi.edu
Published online Oct. 12, 2017.

Cell Culture

The human prostate cancer cell lines PSMA-positive PC3 PIP and PSMA-negative PC3 flu (*9*), the human melanoma cell lines SKMEL3 and MeWo, and the human SCLC cell lines DMS53 and H69 were cultured in RPMI 1640 medium containing 10% fetal bovine serum and 1% penicillin–streptomycin. The human melanoma cell line SKMEL24 was grown in RPMI 1640 medium containing 15% fetal bovine serum, 1 mM sodium pyruvate, 0.1 mM nonessential amino acids, and a 1.5 g/L concentration of sodium bicarbonate. Immortalized normal prostate epithelial RWPE-1 cells were cultured in keratinocyte serum-free medium supplemented with bovine pituitary extract (0.05 mg/mL) and epidermal growth factor (5 ng/mL). All cell lines grown to 80% confluence were used for in vitro and in vivo studies. PSMA expression on PSMA-positive PC3 PIP cells was routinely screened by flow cytometry. SKMEL24, SKMEL3, MeWo, and H69 cell lines were purchased from American Type Culture Collection, cultured for less than 6 mo after resuscitation, and not authenticated. The DMS53 cell line was a gift from Dr. Rajani Ravi of Johns Hopkins and was authenticated in the Johns Hopkins genetic resources facility.

Flow Cytometry

Adherent cells were detached using enzyme-free cell dissociation buffer (Gibco), and suspended cells were harvested by centrifugation. The harvested cells were washed twice with flow cytometry buffer (×1 phosphate-buffered saline with 2 mM ethylenediaminetetraacetic acid and 0.5% fetal bovine serum) and stained with antihuman PSMA antibody conjugated with phycoerythrin (catalog number 341503, clone LNI-17; BioLegend) according to the manufacturer's protocol. PSMA expression was analyzed on a FACSCalibur flow cytometer (Becton Dickinson). Data were analyzed using FlowJo software (Tree Star).

Tumor Models

Animal studies were performed according to protocols approved by the Johns Hopkins University Animal Care and Use Committee. Four- to 6-wk-old male nonobese diabetic severe combined immunodeficiency (NOD/SCID) mice were purchased from the Johns Hopkins Immune-Compromised Mouse Core for in vivo experiments. For tumor generation, 3×10^6 SKMEL3 or MeWo cells were injected subcutaneously in the forward right and left flanks, respectively. SKMEL24 or DMS53 tumor–bearing mice were generated by subcutaneous injection of 5×10^6 cells in separate groups of mice. H69 tumor–bearing mice were generated by tumor passage of a previously snap-frozen H69 tumor. PSMA-positive PC3 PIP and PSMA-PC3 flu tumor–bearing mice were generated by subcutaneous injection of 1×10^6 cells of each line in the forward right and left flanks, respectively. The mice were used in in vivo experiments when the tumors had grown to at least 100–300 mm^3.

Radiosynthesis

The radiosynthesis of the known PSMA imaging agent 2-[3-[1-carboxy-5-(4-^{125}I-iodo-benzoylamino)-pentyl]-ureido]-pentanedioic acid (^{125}I-DCIBzL) was performed as described previously (*9*).

SPECT/CT Imaging

An X-SPECT small-animal SPECT/CT system (Gamma Medica) was used for image acquisition. For each tumor model, 3 mice were used in the imaging studies. After an intravenous injection of 37 MBq (1 mCi) of ^{125}I-DCIBzL, images were acquired at 1 and 24 h after injection. The SPECT projection data were acquired using 2 low-energy, high-resolution parallel-hole collimators with a 6.5-cm radius of rotation. Tomographic data were acquired in 64 projections over 360° at 40 s/projection. After tomography, CT imaging was performed in 512 projections to allow anatomic coregistration. Data were reconstructed using the ordered-subsets expectation maximization algorithm, and volume-rendered images were generated using Amira software (version 5.3.0; Visage Imaging Inc.). For blocking studies, 50 mg/kg of nonradiolabeled DCIBzL were coinjected with radiolabeled ^{125}I-DCIBzL.

Ex Vivo Biodistribution

Tumor-bearing mice received an intravenous injection of 74 kBq (20 μCi) of ^{125}I-DCIBzL. At 1 h after injection, the mice were sacrificed by cervical dislocation, and tumors, blood, heart, lungs, liver, spleen, kidneys, and muscle were collected, weighed, and counted in a γ-counter. Calculation of the percentage injected dose per gram (%ID/g) was based on a standard dose of the injection that was administered to each mouse. At least 4 mice were used per tumor model.

Quantitative Reverse-Transcription Polymerase Chain Reaction (RT-qPCR)

For mRNA extraction, cell lines were cultured to 80% confluence in 10-cm cell culture dishes and lysed using buffer RLT (Qiagen) containing 1:1,000 β-mercaptoethanol. mRNA was extracted from the cell lysate using an RNeasy mini kit (Qiagen) and eluted into 40 μL of RNase-free water. For mRNA extraction, tumors were suspended in buffer RLT containing β-mercaptoethanol and lysed using a microhomogenizer on ice. After homogenization, samples were centrifuged, and the supernatant was used for mRNA extraction as described above. After isolation, samples were quantified for mRNA using the Nanodrop (Thermo Scientific). About 2.5 μg of each mRNA sample were taken to prepare complementary DNA using the high-capacity complementary DNA reverse transcriptase kit (Life Technologies) in a total volume of 50 μL as per the manufacturer's recommended protocol. The resultant complementary DNA samples were used to determine gene expression by RT-qPCR (FOLH1 TaqMan probe; Life Technologies) with GAPDH as an internal control. Relative gene expression was calculated using the ddCt method. FOLH1 expression in cell lines was normalized to the gene expression of the RWPE-1 cells, and that in tumors was normalized to the PSMA-negative PC3 flu tumors.

Western Blot

Tumor samples were homogenized on ice using radioimmunoprecipitation assay buffer (Sigma Aldrich) containing protease inhibitor cocktail and subsequently sonicated to obtain a clear lysate. After centrifugation to remove cell debris, samples were quantified using the bicinchoninic acid protein assay kit (Thermo Fisher Scientific). About 20 μg of each sample were separated on a 10% bis(2-hydroxyethyl) amino-tris(hydroxymethyl)methane gel (Bis-Tris; Life Technologies) and transferred onto a nitrocellulose membrane. The membrane blot was blocked in tris-buffered saline containing 5% milk and 0.05% Tween-20 (ICI Americas, Inc.) for 1 h at room temperature. PSMA protein expression was visualized using anti-PSMA antibody (catalog number 12702S; Cell Signaling) at a concentration of 1:1,000, and β-actin was used as a loading control. For the PSMA-positive PC3 PIP tumor sample, only 2.5 μg of total tumor protein were separated on the gel.

Immunohistochemistry

All tumors were harvested from mice and fixed in 10% buffered formalin, after which they were embedded in paraffin and sectioned at a 5-μm thickness. Tumor sections were deparaffinized using gradient alcohols and hydrated. Antigen retrieval to unmask the epitopes was performed by steaming the slides in 10 mM citrate buffer (pH 6.0) for 20 min, after which they were treated with 3% H_2O_2 solution (Dako) for 10 min. The slides were blocked with 10% fetal bovine serum in phosphate-buffered saline solution for 30 min followed by overnight incubation with prediluted primary anti-PSMA antibody (catalog number N1611; Dako). The slides were washed and then incubated with

secondary universal antibody from the Dako LSAB+ kit (catalog number K0679) for 1 h. Subsequently, 3,3′-diaminobenzidine staining was developed according to the manufacturer's protocol. Sections were counterstained with Gill hematoxylin followed by dehydration with alcohols and xylene and mounted with a cover slip.

Fluorescence Imaging

PSMA-binding IRDye 800CW YC-27 (YC-27) was purchased from LI-COR Biosciences. Tumor-bearing mice were injected with 1 nmol of YC-27, and optical images were acquired on the LI-COR Pearl Impulse near-infrared imager at 24 h after injection. After image acquisition, the animals were sacrificed, their organs (tumors, muscle, liver, spleen, kidneys, stomach, and heart) were assembled on a petri dish, and ex vivo images were acquired. At least 4 mice were imaged per tumor model. For image quantification, regions of interest were drawn over all organs ex vivo, and signal intensity was calculated using the manufacturer's software. Uptake in individual organs was normalized to muscle uptake.

Statistics

Statistical analyses were performed on Prism software (version 6.0; GraphPad). The Student unpaired *t* test was performed to determine statistical significance. All tests were 2-sided, and *P* values of less than 0.05 were considered statistically significant. Error bars in the figures represent ±SEM.

RESULTS

PSMA Expression in Human CCLE Database–Derived and Primary Tumor–Derived TCGA Datasets

We queried PSMA gene expression levels (as *FOLH1*) in the publicly available CCLE database, which contains genomic data from 1,047 cell lines. Prostate cancer cell lines showed the highest PSMA gene expression levels, followed by skin cancer cell lines (Fig. 1A). Nearly 5% of CCLE cell lines showed PSMA gene expression levels higher than the median value of the prostate cancer cell lines, with several cell lines exhibiting at the level of prostate cancer cell lines.

We then investigated PSMA transcript levels in human tumors in TCGA. Transcript expression data from 19 tumor types showed high PSMA levels in prostate cancers followed by cancers of the kidney, liver, and urothelium (Fig. 1B and Supplemental Table 1; supplemental materials are available at http://jnm.snmjournals.org). Nearly 97% of prostate cancers exhibited PSMA transcripts, and 12% of all the nonprostatic tumors showed PSMA transcripts similar to or above the first quartile of prostate tumor transcript levels. Of those, about 10% were contributed by kidney, liver, urothelium, squamous lung, and melanoma tumors, with the remaining 1.4% representing all other cancers. Further analysis of individual cancer types showed that 57% of kidney, 39% of liver, 26% of urothelium, 21% of low-grade glioma, 11.8% of lung squamous cell carcinoma, and 9% of skin cancers demonstrated PSMA transcript levels in the above-mentioned range. Overall, high PSMA transcript levels were observed to be a nonfrequent event in nonprostatic cancers. These data indicate that PSMA is expressed in a variety of nonprostatic cancer epithelial cell lines and in tumors, albeit at a lower frequency than that of prostate.

Validation of PSMA Expression in Nonprostatic Cancer Cell Lines and Xenografts

To validate the PSMA positivity noted in the nonprostatic cancer cell lines in CCLE, we selected several that were either high (SKMEL24, SKMEL3, DMS53) or low (Mewo, H69) in PSMA expression and performed RT-qPCR and flow cytometry for gene and cell-surface expression, respectively. RT-qPCR

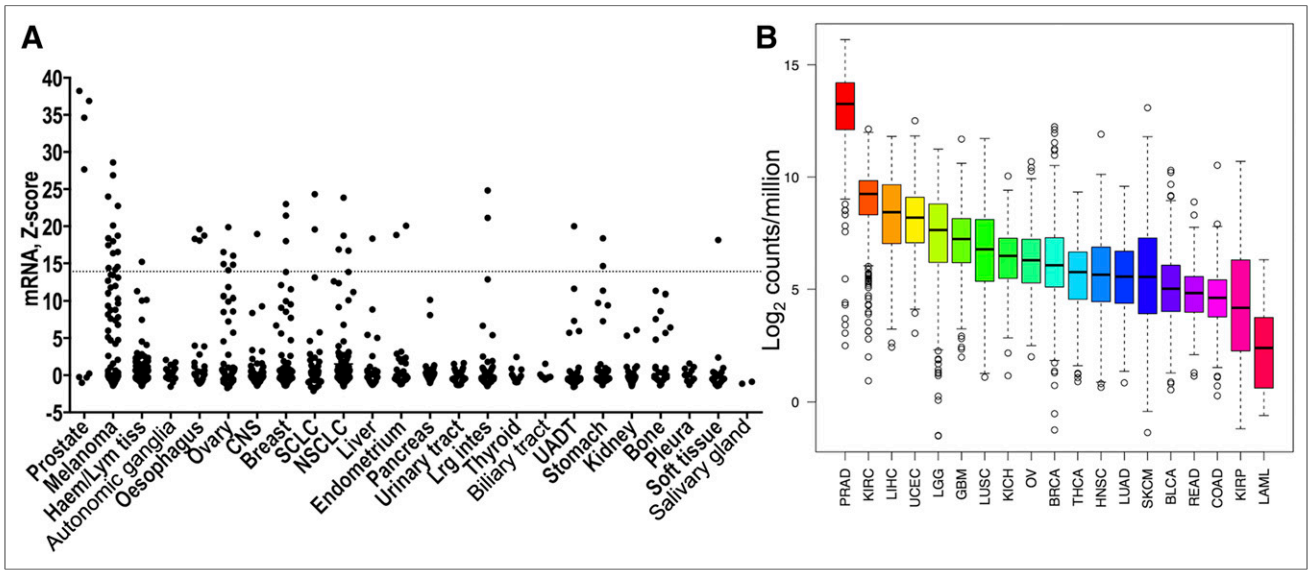

FIGURE 1. PSMA expression in human tumors. (A) *FOLH1* gene expression in cell lines extracted from CCLE database, converted into *z* score, and plotted on the basis of cancer type. Dot plot with line at median value of prostate cancer cell lines is shown. (B) Expression of *FOLH1* in different tissue types from TCGA RNA-Seq version 2 data. Dots on top and bottom of box represent outliers. Bars at top and bottom of box represent minimum and maximum expression values of *FOLH1* gene, excluding outliers. Box represents 50% of samples. Horizontal bold line inside box is median *FOLH1* expression in disease type. CNS = central nervous system; NSCLC = non–small cell lung carcinoma; UADT = upper aerodigestive tract; PRAD = prostate adenocarcinoma; KIRC = kidney renal clear cell carcinoma; LIHC = liver hepatocellular carcinoma; UCEC = uterine corpus endometrial carcinoma; LGG = brain lower-grade glioma; GBM = glioblastoma multiforme; LUSC = lung squamous cell carcinoma; KICH = kidney chromophobe; OV = ovarian carcinoma; BRCA = breast invasive carcinoma; THCA = thyroid carcinoma; HNSC = head and neck squamous cell carcinoma; LUAD = lung adenocarcinoma; SKCM = skin cutaneous melanoma; BLCA = bladder urothelial carcinoma; READ = rectum adenocarcinoma; COAD = colon adenocarcinoma; KIRP = kidney renal papillary cell carcinoma; LAML = acute myeloid leukemia.

results showed that SKMEL24, SKMEL3, and DMS53 cells were PSMA-positive, with the highest PSMA expression levels being in SKMEL24 and SKMEL3, followed by DMS53 (Fig. 2A). MeWo and H69 were negative for PSMA. Notably, PSMA expression in melanoma (SKMEL24, SKMEL3) and lung cells (DMS53) was considerably lower than that in prostate cells, reflecting the CCLE data. PSMA positivity in these cell lines was also confirmed in flow cytometric analyses, which showed PSMA expression in nonprostatic cells to be 2–3 orders of magnitude lower than that in LNCap control cells (Fig. 2B), which overexpress copious amounts of PSMA (*10*). We next sought to confirm that PSMA expression was maintained in vivo. In subcutaneous xenograft tumors, PSMA expression was detected in SKMEL24, SKMEL3, and DMS53 tumors by RT-qPCR (Fig. 2C) and Western blot (Fig. 2D). Gene and protein expression analyses of the tumors showed the highest PSMA expression levels to be in SKMEL24 and DMS53, followed by SKMEL3. The observed PSMA levels were also several orders of magnitude lower than those observed in PSMA-positive PC3 PIP tumors. Collectively, data from melanoma and SCLC cell lines demonstrated cell-surface PSMA expression on epithelial cells of nonprostatic cancers.

Imaging PSMA Expression in Nonprostate Cancer Xenografts by SPECT Imaging

We then investigated whether PSMA expression in nonprostatic tumors is sufficiently high for noninvasive detection by PSMA-binding imaging agents.

Validation in Melanoma Models. We inoculated SKMEL24 cells subcutaneously into male mice and allowed tumors to become established. SPECT imaging of those mice at 60 min after injection of ^{125}I-DCIBzL, an established PSMA SPECT imaging agent, showed accumulation and retention of radioactivity in the SKMEL24 tumors. Imaging at 24 h after injection of ^{125}I-DCIBzL also demonstrated retention of radioactivity in the tumors (Fig. 3A). Accumulation of radioactivity in the tumors could be blocked by coinjection of the nonradiolabeled compound, confirming PSMA-mediated uptake.

We next investigated whether graded levels of PSMA expression could be imaged with PSMA-targeted imaging agents. To test this, we selected the SKMEL3 cell line, with moderate expression of PSMA, and the MeWo cell line, which does not express PSMA. SPECT imaging of mice harboring tumors showed specific but low accumulation of radioactivity in SKMEL3 tumors and almost no radiotracer uptake in MeWo tumors (Fig. 3B). Liver and kidney could also be clearly visualized, in line with previous studies (*9*). Further corroborating the imaging, biodistribution studies demonstrated graded radiotracer uptake in the tumors in proportion to the level of expression of PSMA in each cell line; namely, SKMEL24 > SKMEL3 > MeWo. The %ID/g for SKMEL24, SKMEL3, and MeWo tumors was 14.3 ± 1.5, 9.3 ± 0.4, and 1.2 ± 0.1, respectively. In mice that received a blocking dose, the %ID/g for SKMEL24, SKMEL3, and MeWo tumors was 1.7 ± 0.1, 1.1 ± 0.1, and 0.9 ± 0.1, respectively, indicating PSMA-mediated binding in the SKMEL24 and SKMEL3 tumor models (Fig. 3C). For

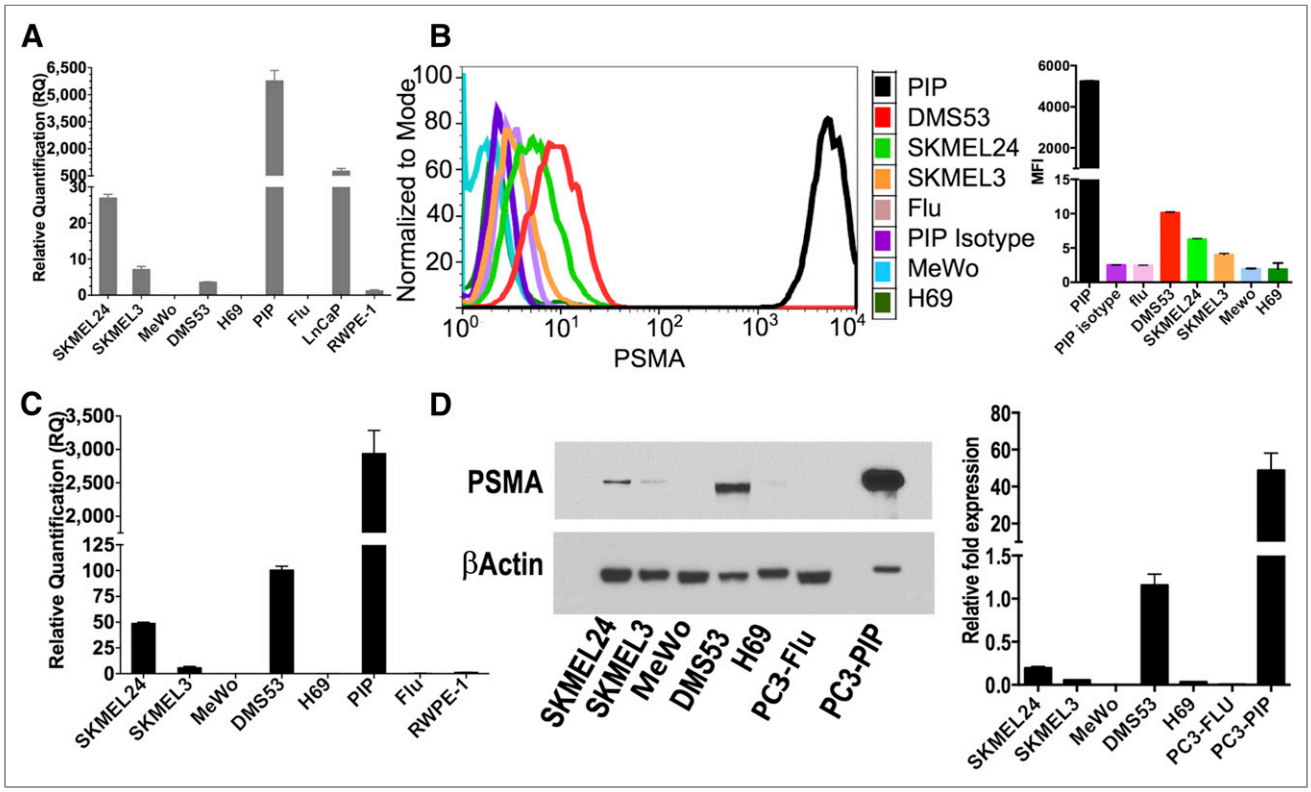

FIGURE 2. Validation of PSMA expression in nonprostatic human cancer cell lines and xenografts. (A) PSMA gene expression in selected melanoma and lung cancer cell lines. (B) Flow cytometry of PSMA surface expression in PSMA-positive PC3 PIP, PSMA-negative PC3 flu, and nonprostatic cancer cell lines. PSMA-positive PC3 PIP is designed to overexpress copious amounts of PSMA. Mean fluorescence intensity quantification shows that PSMA-positive PC3 PIP has high level of PSMA surface expression whereas PSMA-negative PC3 flu, MeWo, and H69 are negative and DMS53, SKMEL24, and SKMEL3 are positive (right panel). (C) PSMA gene expression in selected melanoma and lung cancer xenografts. (D) PSMA total protein levels in selected melanoma and lung cancer xenografts and densitometric quantification (right panel).

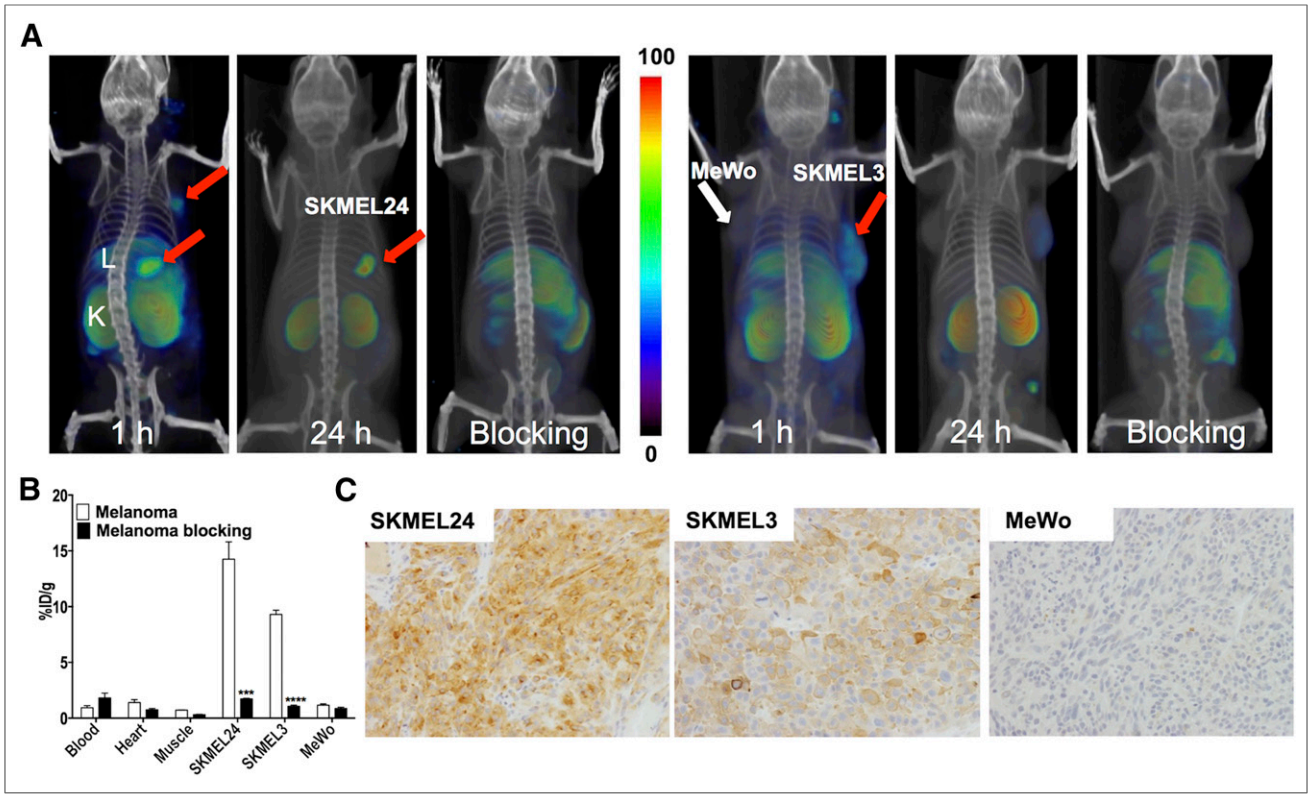

FIGURE 3. PSMA imaging in subcutaneous melanoma xenografts with known PSMA-specific radiotracer, ^{125}I-DCIBzL. (A) Male NOD/SCID mice bearing SKMEL24 xenografts or SKMEL3 and MeWo were injected with 37 MBq (1 mCi) of ^{125}I-DCIBzL through tail vein, and SPECT/CT images were acquired 1 and 24 h later. Arrows = tumor; L = liver; K = kidney. (B) Mice harboring SKMEL24 or SKMEL3 and MeWo xenografts were administered 74 kBq (20 μCi) of ^{125}I-DCIBzL via tail vein injection, and biodistribution studies were performed 1 h afterward. For blocking dose, DCIBzL at 50 mg/kg was injected subcutaneously 30 min before ^{125}I-DCIBzL. Data are mean ± SEM of 4 animals. Significance of value is indicated by asterisks, and comparative reference is blocking dose uptake in same tumor. ***$P < 0.001$. ****$P < 0.0001$. (C) Representative microscopic images of PSMA-stained sections from same cohort of mice obtained at ×20 magnification.

molecular pathologic validation, biodistribution data in melanoma xenografts were confirmed by PSMA immunohistochemical analysis, which demonstrated intense and moderate PSMA immunoreactivity in SKMEL24 and SKMEL3 tumors, respectively. MeWo tumors did not show PSMA immunoreactivity (Fig. 3D). We have not observed PSMA immunoreactivity in the vasculature of these xenografts.

As additional positive and negative controls, we performed biodistribution studies in PSMA-positive PC3 PIP and PSMA-negative PC3 flu tumors. ^{125}I-DCIBzL uptake in the PSMA-positive PC3 PIP tumors was 29.9 ± 3.9, and that in the PSMA-negative PC3 flu tumors was 1.8 ± 0.4, further supporting the validity of the imaging agent (Supplemental Fig. 1).

Confirmation in SCLC Models. We next sought to confirm our observations in melanoma in a different tumor type. We chose the SCLC cell line DMS53, which is highly PSMA-positive, and the cell line H69, which is PSMA-negative. SPECT imaging of NOD/SCID mice bearing DMS53 tumors showed specific accumulation of radioactivity in tumors by 60 min that persisted at 24 h (Figs. 4A and 4B). Reduced radioactivity uptake was observed in the DMS53 tumors in the blocking study, demonstrating PSMA-specific binding (Fig. 4A). No appreciable accumulation of radioactivity was observed in PSMA-negative H69 tumors. The %ID/g observed in the biodistribution studies was 5.8 ± 0.7 and 0.9 ± 0.0 for DMS53 and H69 tumors, respectively. In mice receiving a blocking dose, the %ID/g was 0.8 ± 0.1 and 0.7 ± 0.1 for DMS53 and H69 tumors, respectively, indicating PSMA-mediated uptake in the former (Fig. 4C). Confirming the imaging and biodistribution studies, immunohistochemical analysis demonstrated moderate PSMA immunoreactivity in DMS53 tumors. PSMA immunoreactivity in H69 tumors was undetectable (Fig. 4D).

Collectively, these imaging, biodistribution, and blocking studies demonstrated that PSMA expression in some of the nonprostatic tumors is sufficiently expressed in the epithelial cells to be visualized by existing imaging agents.

Validation of PSMA Expression in Skin and Lung Cancer Xenografts by Near-Infrared Optical Imaging

Optical imaging agents are being exploited to develop photodynamic therapy, and several low-molecular-weight PSMA-binding near-infrared optical imaging agents have been reported (*11–13*). One such agent, YC-27, previously reported by us, provides high target-to-nontarget imaging specificity 24 h after injection. To investigate the feasibility of using PSMA-targeted optical imaging agents for detecting and targeting tumors with lower levels of PSMA expression, such as melanoma, we performed near-infrared imaging on mice bearing subcutaneous PSMA-positive SKMEL24 and SKMEL3 tumors, and PSMA-negative MeWo tumors, 24 h after injection of YC-27. Results demonstrated significant accumulation of fluorescent signal in the SKMEL24 tumors and little to none in the

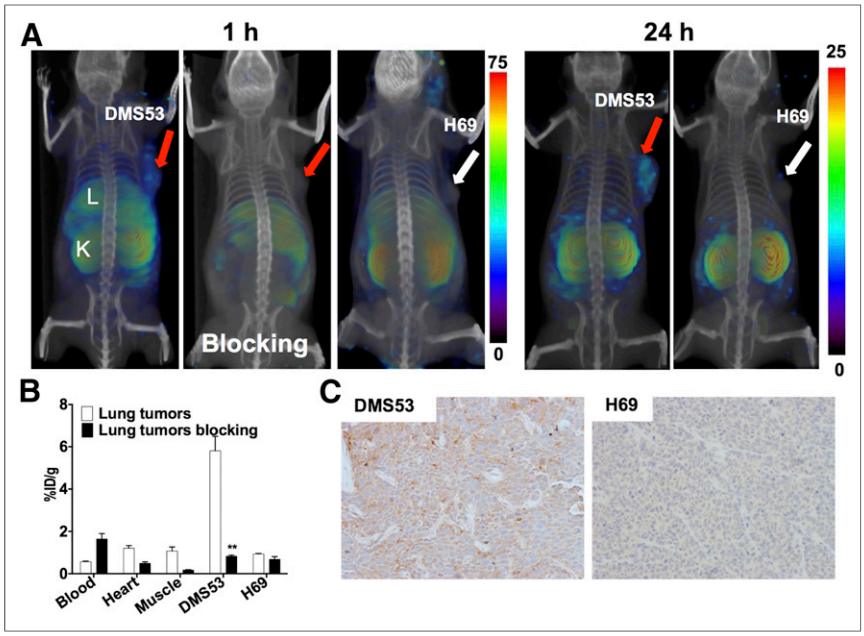

FIGURE 4. PSMA imaging in subcutaneous lung cancer xenografts with known PSMA-specific radiotracer, ^{125}I-DCIBzL. (A) Male NOD/SCID mice bearing DMS53 or H69 xenografts were administered 37 MBq (1 mCi) of ^{125}I-DCIBzL via tail vein injection, and SPECT/CT images were acquired 1 h and 24 h (right panels) afterward. Arrows = tumor; L = liver; K = kidney. (B) Mice harboring DMS53 or H69 xenografts were administered 74 kBq (20 μCi) of ^{125}I-DCIBzL, and biodistribution studies were performed 1 h afterward. For blocking dose, DCIBzL at 50 mg/kg was coinjected with ^{125}I-DCIBzL. Data are mean ± SEM of 4 animals. Significance of value is indicated by asterisks, and comparative reference is blocking dose uptake in same tumor. $^{**}P < 0.01$. (C) Representative microscopy images of PSMA-stained sections from same cohort of mice obtained at ×20 magnification.

melanotic SKMEL3 tumors (due to quenching) and PSMA-negative MeWo tumors. Similarly, in SCLC xenograft models, high fluorescence intensity was observed in PSMA-positive DMS53 tumors but not in PSMA-negative H69 tumors (Fig. 5A). These qualitative observations were further supported by quantification of the fluorescence intensity of dissected tumors, which showed a significant increase in PSMA-positive tumors (Fig. 5B).

DISCUSSION

PSMA expression in the tumor neovasculature of nonprostatic tumors is known and used for imaging and therapeutic purposes; however, its expression in epithelial cells of nonprostatic cancer has not been well characterized. By harnessing large-scale genomic data, we showed that nonprostatic cancer cell lines in the CCLE database have high PSMA gene expression. These observations in cell lines were supported by analysis of patient tumor–derived TCGA data. High PSMA transcript levels in nonprostatic cancers occurred at a low frequency, and observed levels were similar to first-quartile transcript levels in prostate cancers. We selected a few PSMA-positive melanoma and SCLC cell lines from the CCLE, confirmed PSMA expression in cultured cells and subcutaneous xenografts, and demonstrated the potential of PSMA-targeting nuclear and optical agents to detect this expression. These results establish nonprostatic tumor models with epithelial cell PSMA expression and demonstrate that PSMA expression was sufficiently high for tumor targeting and imaging.

High-throughput sequencing has made precision medicine a reality (*14*). The availability of RNA sequencing data from many cancer cell lines has allowed us to profile PSMA gene expression in various cancer cell lines. Although prostate cancer cell lines showed high gene expression levels as anticipated, skin cancer cell lines were second highest. Notably, PSMA gene expression, although less frequent, was observed in many nonprostatic cell lines at a level like that of the prostate cancer cell lines. Several studies showed that protein levels and function are poorly predicted by genomic and transcriptomic analysis of patient-derived tumors, suggesting that further confirmation of protein expression and function is warranted even in cell lines expressing abundant transcript (*15*). In the limited number of cell lines we investigated, 8 in total, there was a strong correlation of PSMA transcript level with protein expression suggesting that transcript analysis could be indicative of PSMA expression in the tumors. These observations provide opportunities to tailor transcript data acquired from patient biopsies with existing PSMA imaging and therapeutics.

PSMA-targeted imaging and therapeutic agents are making significant strides in prostate cancer diagnosis and treatment (*16–21*). However, despite the availability of excellent imaging agents (*22*) and the expression of PSMA in most solid-tumor neovasculature, PSMA-targeted imaging has largely been limited to prostate cancer (*7,8,23,24*). Clinical case reports demonstrating PSMA expression in other cancers are appearing (*25–27*), although larger prospective trials that would confirm the clinical utility of PSMA agents in nonprostatic cancers have yet to be reported. Validation of existing PSMA imaging and therapeutic agents in nonprostatic tumors has been hampered by the lack of suitable models. Our results provide PSMA-positive nonprostatic xenograft models for further validation of those imaging agents.

Because of the elevated expression of PSMA in prostate cancer, it has been leveraged as a diagnostic, drug-delivery, and immunomodulatory target for this disease (*28–30*). Several PSMA-targeted imaging and radiotherapeutic agents are under investigation for use in prostate cancer (*30–33*). ^{177}Lu-labeled J591 anti-PSMA antibody and several low-molecular-weight agents are now in clinical trials for treating micrometastases (*34*). PSMA expression levels in tested nonprostatic cell lines and tumors is nearly 30-fold less than that observed in LNCaP cells, suggesting that radiotherapeutic alternatives for tumors derived from these nonprostatic cells may be challenging but worth investigating. Previous studies using ^{111}In-J591 to specifically target the tumor neovasculature has shown promising results in kidney, bladder, lung, breast, colorectal, and pancreatic cancers and in melanoma (*35*). Although earlier immunohistochemical analysis studies reported a lack of PSMA expression on the epithelial cells, a few recent studies reported PSMA expression on the epithelial cells of nonprostatic tumors and metastatic nodules (*26,36*). PSMA-targeted optical imaging agents are also being investigated as theranostic photosensitizers to deliver photodynamic therapy to prostate tumor xenografts (*37*). Our observations using PSMA optical imaging agents and their specific accumulation in PSMA-positive nonprostatic tumor xenografts suggest a role for such agents in other

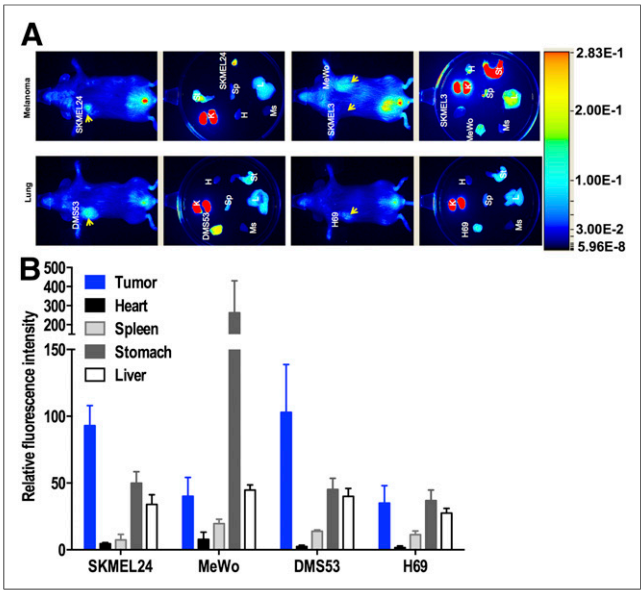

FIGURE 5. Near-infrared fluorescence imaging of PSMA expression in subcutaneous melanoma and lung xenografts with YC-27. (A) Male NOD/SCID mice bearing melanoma and lung xenografts were administered 1 nmol of a near-infrared–labeled PSMA-targeting reagent, YC-27, via tail vein injection, and fluorescence images were acquired 24 h afterward. (B) After near-infrared imaging, selected tissues were harvested and fluorescence intensity was measured and normalized to muscle fluorescence intensity. Arrow = tumor; H = heart; K = kidney; L = liver; Ms = muscle; Sp = spleen; St = stomach.

tumor types. Taken together, our data show that PSMA expression in nonprostatic tumors is sufficiently high to be detected by existing PSMA imaging agents.

Recently, a PSMA-targeted imaging agent was used to detect metastatic nodules in a patient with clear cell renal carcinoma, although validation of PSMA expression by immunohistochemical analysis was not reported (*38*). Although PSMA-targeted therapeutics are being investigated and have shown therapeutic efficacy in patients with prostate cancer (*33,35,39*), their benefit for other cancers is not established. Melanoma and SCLC tumor models described in this work will provide an opportunity to evaluate these agents in preclinical models of nonprostatic cancers. Beyond any potential diagnostic utility, new theranostic treatment paradigms using PSMA-targeted endoradiotherapy may prove to be of particular value in diseases difficult to treat, such as metastatic melanoma and SCLC.

CONCLUSION

We have demonstrated that PSMA is endogenously expressed in nonprostatic cancer cell lines and that expression in melanoma and SCLC is sufficiently high to be visualized using existing PSMA imaging agents. Also, we showed that graded levels of PSMA expression in nonprostatic cancer xenografts can be imaged using both nuclear and optical imaging agents. Our data suggest that certain nonprostatic tumors may express PSMA directly on the cancer cells, in addition to that previously reported in neovasculature.

DISCLOSURE

Grant support was received from the National Institutes of Health (R01CA134675, U01 CA183031, P41 EB024495, and R01 CA184228 to Martin G. Pomper) and the Allegheny–Hopkins Network Cancer Research Fund and R01 CA166131 (to Sridhar Nimmagadda). No other potential conflict of interest relevant to this article was reported.

REFERENCES

1. Davis MI, Bennett MJ, Thomas LM, Bjorkman PJ. Crystal structure of prostate-specific membrane antigen, a tumor marker and peptidase. *Proc Natl Acad Sci USA*. 2005;102:5981–5986.
2. Pavlícek J, Ptacek J, Bařinka C. Glutamate carboxypeptidase II: an overview of structural studies and their importance for structure-based drug design and deciphering the reaction mechanism of the enzyme. *Curr Med Chem.* 2012;19:1300–1309.
3. Bařinka C, Rojas C, Slusher B, Pomper M. Glutamate carboxypeptidase II in diagnosis and treatment of neurologic disorders and prostate cancer. *Curr Med Chem.* 2012;19:856–870.
4. Sweat SD, Pacelli A, Murphy GP, Bostwick DG. Prostate-specific membrane antigen expression is greatest in prostate adenocarcinoma and lymph node metastases. *Urology.* 1998;52:637–640.
5. Bostwick DG, Pacelli A, Blute M, Roche P, Murphy GP. Prostate specific membrane antigen expression in prostatic intraepithelial neoplasia and adenocarcinoma: a study of 184 cases. *Cancer.* 1998;82:2256–2261.
6. Ghosh A, Heston WD. Tumor target prostate specific membrane antigen (PSMA) and its regulation in prostate cancer. *J Cell Biochem.* 2004;91:528–539.
7. Chang SS, O'Keefe DS, Bacich DJ, Reuter VE, Heston WD, Gaudin PB. Prostate-specific membrane antigen is produced in tumor-associated neovasculature. *Clin Cancer Res.* 1999;5:2674–2681.
8. Chang SS, Reuter VE, Heston WD, Bander NH, Grauer LS, Gaudin PB. Five different anti-prostate-specific membrane antigen (PSMA) antibodies confirm PSMA expression in tumor-associated neovasculature. *Cancer Res.* 1999;59:3192–3198.
9. Chen Y, Foss CA, Byun Y, et al. Radiohalogenated prostate-specific membrane antigen (PSMA)-based ureas as imaging agents for prostate cancer. *J Med Chem.* 2008;51:7933–7943.
10. Kiess AP, Minn I, Chen Y, et al. Auger radiopharmaceutical therapy targeting prostate-specific membrane antigen. *J Nucl Med.* 2015;56:1401–1407.
11. Chen Y, Dhara S, Banerjee SR, et al. A low molecular weight PSMA-based fluorescent imaging agent for cancer. *Biochem Biophys Res Commun.* 2009;390:624–629.
12. Kelderhouse LE, Chelvam V, Wayua C, et al. Development of tumor-targeted near infrared probes for fluorescence guided surgery. *Bioconjug Chem.* 2013;24:1075–1080.
13. Lütje S, Rijpkema M, Goldenberg DM, et al. Pretargeted dual-modality immuno-SPECT and near-infrared fluorescence imaging for image-guided surgery of prostate cancer. *Cancer Res.* 2014;74:6216–6223.
14. Le DT, Uram JN, Wang H, et al. PD-1 blockade in tumors with mismatch-repair deficiency. *N Engl J Med.* 2015;372:2509–2520.
15. Akbani R, Ng PK, Werner HM, et al. A pan-cancer proteomic perspective on The Cancer Genome Atlas. *Nat Commun.* 2014;5:3887.
16. Szabo Z, Mena E, Rowe SP, et al. Initial evaluation of [^{18}F]DCFPyL for prostate-specific membrane antigen (PSMA)-targeted PET imaging of prostate cancer. *Mol Imaging Biol.* 2015;17:565–574.
17. Rowe SP, Gage KL, Faraj SF, et al. ^{18}F-DCFBC PET/CT for PSMA-based detection and characterization of primary prostate cancer. *J Nucl Med.* 2015;56:1003–1010.
18. Rowe SP, Macura KJ, Ciarallo A, et al. Comparison of prostate-specific membrane antigen-based ^{18}F-DCFBC PET/CT to conventional imaging modalities for detection of hormone-naive and castration-resistant metastatic prostate cancer. *J Nucl Med.* 2016;57:46–53.
19. Vallabhajosula S, Nikolopoulou A, Jhanwar YS, et al. Radioimmunotherapy of metastatic prostate cancer with ^{177}Lu-DOTAhuJ591 anti prostate specific membrane antigen specific monoclonal antibody. *Curr Radiopharm.* 2016;9:44–53.
20. Weineisen M, Schottelius M, Simecek J, et al. ^{68}Ga- and ^{177}Lu-labeled PSMA I&T: optimization of a PSMA-targeted theranostic concept and first proof-of-concept human studies. *J Nucl Med.* 2015;56:1169–1176.
21. Kratochwil C, Giesel FL, Stefanova M, et al. PSMA-targeted radionuclide therapy of metastatic castration-resistant prostate cancer with Lu-177 labeled PSMA-617. *J Nucl Med.* 2016;57:1170–1176.
22. Mease RC, Foss CA, Pomper MG. PET imaging in prostate cancer: focus on prostate-specific membrane antigen. *Curr Top Med Chem.* 2013;13:951–962.
23. Baccala A, Sercia L, Li J, Heston W, Zhou M. Expression of prostate-specific membrane antigen in tumor-associated neovasculature of renal neoplasms. *Urology.* 2007;70:385–390.

24. Haffner MC, Kronberger IE, Ross JS, et al. Prostate-specific membrane antigen expression in the neovasculature of gastric and colorectal cancers. *Hum Pathol.* 2009;40:1754–1761.
25. Pandit-Taskar N, O'Donoghue JA, Divgi CR, et al. Indium 111-labeled J591 anti-PSMA antibody for vascular targeted imaging in progressive solid tumors. *EJNMMI Res.* 2015;5:28.
26. Nomura N, Pastorino S, Jiang P, et al. Prostate specific membrane antigen (PSMA) expression in primary gliomas and breast cancer brain metastases. *Cancer Cell Int.* 2014;14:26.
27. Denmeade SR, Mhaka AM, Rosen DM, et al. Engineering a prostate-specific membrane antigen-activated tumor endothelial cell prodrug for cancer therapy. *Sci Transl Med.* 2012;4:140ra86.
28. DiPippo VA, Olson WC, Nguyen HM, Brown LG, Vessella RL, Corey E. Efficacy studies of an antibody-drug conjugate PSMA-ADC in patient-derived prostate cancer xenografts. *Prostate.* 2015;75:303–313.
29. Slovin SF, Kehoe M, Durso R, et al. A phase I dose escalation trial of vaccine replicon particles (VRP) expressing prostate-specific membrane antigen (PSMA) in subjects with prostate cancer. *Vaccine.* 2013;31:943–949.
30. Cho SY, Gage KL, Mease RC, et al. Biodistribution, tumor detection, and radiation dosimetry of ^{18}F-DCFBC, a low-molecular-weight inhibitor of prostate-specific membrane antigen, in patients with metastatic prostate cancer. *J Nucl Med.* 2012;53:1883–1891.
31. Eiber M, Maurer T, Souvatzoglou M, et al. Evaluation of hybrid ^{68}Ga-PSMA ligand PET/CT in 248 patients with biochemical recurrence after radical prostatectomy. *J Nucl Med.* 2015;56:668–674.
32. Zechmann CM, Afshar-Oromieh A, Armor T, et al. Radiation dosimetry and first therapy results with a ^{124}I/^{131}I-labeled small molecule (MIP-1095) targeting PSMA for prostate cancer therapy. *Eur J Nucl Med Mol Imaging.* 2014;41:1280–1292.
33. Tagawa ST, Milowsky MI, Morris M, et al. Phase II study of lutetium-177-labeled anti-prostate-specific membrane antigen monoclonal antibody J591 for metastatic castration-resistant prostate cancer. *Clin Cancer Res.* 2013;19:5182–5191.
34. Afshar-Oromieh A, Babich JW, Kratochwil C, et al. The rise of PSMA ligands for diagnosis and therapy of prostate cancer. *J Nucl Med.* 2016;57(suppl):79S–89S.
35. Milowsky MI, Nanus DM, Kostakoglu L, et al. Vascular targeted therapy with anti-prostate-specific membrane antigen monoclonal antibody J591 in advanced solid tumors. *J Clin Oncol.* 2007;25:540–547.
36. Kinoshita Y, Kuratsukuri K, Landas S, et al. Expression of prostate-specific membrane antigen in normal and malignant human tissues. *World J Surg.* 2006;30:628–636.
37. Chen Y, Chatterjee S, Lisok A, et al. A PSMA-targeted theranostic agent for photodynamic therapy. *J Photochem Photobiol B.* 2017;167:111–116.
38. Demirci E, Ocak M, Kabasakal L, et al. ^{68}Ga-PSMA PET/CT imaging of metastatic clear cell renal cell carcinoma. *Eur J Nucl Med Mol Imaging.* 2014;41:1461–1462.
39. Morris MJ, Divgi CR, Pandit-Taskar N, et al. Pilot trial of unlabeled and indium-111-labeled anti-prostate-specific membrane antigen antibody J591 for castrate metastatic prostate cancer. *Clin Cancer Res.* 2005;11:7454–7461.